Research Square

Preprints are preliminary reports that have not undergone peer review.
They should not be considered conclusive, used to inform clinical practice,
or referenced by the media as validated information.

Monochromatic Ultra-Slow Oscillations (MUSO, ~ 0.1 Hz) in EEG: topography, interparticipant variabilities and relation to higher frequency oscillations

Firat Sansal

firat.sansal@charite.de

Charité - Universitätsmedizin Berlin

Deniz Kumral

University of Freiburg

Tim Paul Steinfath

Max Planck Institute for Human Cognitive and Brain Sciences

Juanli Zhang

University of Geneva

Michael Gaebler

Max Planck Institute for Human Cognitive and Brain Sciences

Arno Villringer

Max Planck Institute for Human Cognitive and Brain Sciences

Vadim Nikulin

Department of Neurology, Max Planck Institute for Human Cognitive and Brain Sciences, Leipzig, Germany

Article

Keywords: MUSO, cross-frequency coupling, EEG, vasomotion, neuronal oscillations

Posted Date: November 10th, 2026

DOI: https://doi.org/10.21203/rs.3.rs-11397919/v1

License: This work is licensed under a Creative Commons Attribution 4.0 International License.
Read Full License

Additional Declarations: No competing interests reported.

Monochromatic Ultra-Slow Oscillations (MUSO, ~ 0.1 Hz) in EEG: topography, interparticipant variabilities and relation to higher frequency oscillations

Firat Sansal[1,6*], Deniz Kumral[2,7], Paul Steinfath[1,4], Juanli Zhang[1,3], Michael Gaebler[1], Arno Villringer[1,5**], Vadim V. Nikulin[1**]

[1]Department of Neurology, Max Planck Institute for Human Cognitive and Brain Sciences, Leipzig, Germany

[2] Institute of Psychology, Neuropsychology, University of Freiburg, Germany

[3]University Hospitals and Faculty of Medicine, University of Geneva, Geneva, Switzerland

[4]International Max Planck Research School NeuroCom, Leipzig, Germany

[5] Department of Cognitive Neurology, University Hospital Leipzig, Leipzig, Germany

[6] International Graduate Program Medical Neurosciences, Charité-Universitätsmedizin, Berlin, Germany

[7]BrainLinks-BrainTools, University of Freiburg, Freiburg im Breisgau, Germany

* corresponding author: firat.sansal@charite.de

** equal to senior authorship

ABSTRACT

While magneto- and electroencephalography studies typically focus on signals above 1 Hz, processes with frequencies below 0.2 Hz remain largely unexplored. Here, we systematically characterized Monochromatic Ultra-Slow Oscillations (MUSO)—a narrow-band activity centered at approximately 0.1 Hz—in a large cohort (n=175). Using two reference schemes and a modified relative periodic power (rPP) metric, we accurately quantified its periodicity. MUSO was invariant to eyes-open versus eyes-closed conditions but displayed significant demographic differences: female participants presented elevated rPP compared with males, and older adults (55–75 years) presented marked rPP reductions relative to younger cohorts (20–35 years), predominantly in the parietal and occipital regions. Cross-frequency coupling further distinguished MUSO from conventional infraslow fluctuations (ISFs), despite overall sparse phase–amplitude coupling with standard neuronal rhythms (1–45 Hz). Collectively, our results establish the MUSO as a distinct electrophysiological phenomenon separate from aperiodic background activity. Because its properties are inconsistent with those of global respiratory or systemic blood pressure artifacts, we propose the MUSO as a noninvasive electrical readout of localized cerebral vasomotion. These results provide a framework for tracking neurovascular coupling and suggest that MUSO dynamics could serve as a functional biomarker of age-related cerebrovascular remodeling.

Keywords: MUSO, cross-frequency coupling, EEG, vasomotion, neuronal oscillations.

1. INTRODUCTION

Infraslow EEG activity: conceptual advances and technical challenges

Neural dynamics operate on many timescales, reflecting distinct mechanisms, and previous research has focused primarily on neuronal signals above 0.2 Hz. However, a number of studies using electroencephalography (EEG) have revealed that brain activity occurs at longer timescales and is characterized by frequencies below 0.2 Hz [1–4]. Diverse terminology has been used for electrophysiological activity below 0.2 Hz, such as “infraslow fluctuations” (ISF) for the range of <0.1 Hz [5] or 0.01–0.1 Hz [6] and the term “infraslow oscillations” (ISO) for frequencies in the range of 0.02–0.2 Hz [7], <0.1 Hz [8], <0.02 Hz [9], or 0.05–0.099 Hz [10] and “very low frequency oscillations” (VLFO) for the range of <0.2 Hz [11]. Despite growing interest in these slow oscillations [6,12–14], their analysis remains challenging because of the need for longer recording durations and their sensitivity to artifacts such as head movement, eye blinking, and electrode–skin impedance issues [4]. These challenges in methodology and signal processing make it difficult to study signals below 0.2 Hz, thereby hindering our understanding of the physiological basis of these oscillations.

Contrasting Scale-Free and Periodic Dynamics in Infraslow EEG Signals

EEG signals have been reported in two primary types of activities, aperiodic and periodic, each with distinct functional implications and underlying mechanisms [15,16]. On the one hand, irregular, arrhythmic brain activity often follows scale-free dynamics, meaning that it lacks a characteristic timescale and a peak in the frequency domain. Such activity is usually quantified by fitting a power-law function to the power spectrum of the data [17–21]. On the other hand, for periodic activity of EEG signals below 0.2 Hz, reports and estimates have been inconsistent. In theory, periodic activity is expected to show a salient peak at power spectra for considerable time intervals. Periodic, nearly sinusoidal infraslow oscillations were first observed by Aladjalova et al. [22] in rabbits via invasive cortical recordings. These activities were found both in frontal and occipital areas and were characterized by a periodic pattern (e.g., rhythmic oscillations) with 1–2 cycles/min and 7–9 cycles/min corresponding to 0.016–0.032 Hz and 0.11–0.15 Hz, respectively. Similar ~0.1 Hz rhythms have been anecdotally described in human electrophysiology [23–25], but these observations were largely based on visual inspection rather than systematic spectral analysis, whereas others emphasize the absence of prominent peaks in EEG spectra below 0.5 Hz [5,17,26]. Nikulin et al. [27] used multimodal measurements, including EEG, functional near infrared spectroscopy (fNIRS), continuous arterial blood pressure, respiration, and skin laser Doppler recordings, to comprehensively describe EEG oscillations with a pronounced peak in the range of 0.07–0.14 Hz. Because they occur in a very narrow frequency range, these oscillations were termed “Monochromatic Ultra-Slow Oscillations” (MUSO). The MUSO term emphasizes their pronounced, narrow spectral peak, which translates to near-perfect sinusoidal signals in the time domain and separates them from the relatively broadband fluctuations typical for signals with a 1/f spectrum. Nikulin et al. [27] characterized these oscillations and linked them to diverse hemodynamic signals, fNIRS and arterial blood pressure signals and concluded that MUSO most likely reflects an electrical counterpart of cerebral vasomotion.

Regardless of the debate in terms of the periodicity, rhythmicity or terminology of slow EEG oscillations (for reviews, see [2–4]), EEG signals of approximately <0.2 Hz have been associated with the amplitude of faster neuronal activities in sleeping adult participants [7,28], in task-performing participants [5], and in patients in postanoxic coma [29]. These results

relate infraslow EEG signals to cortical excitability, which in turn influences diverse neuronal processes in the healthy and pathological brain, including sleep (or consciousness), perception, cognition, and motor control [2]. In addition, infraslow EEG signals have been shown to be correlated with resting-state network dynamics (BOLD fMRI), suggesting a role in synchronizing network activity across distributed areas of the neocortex [6,30].

Unresolved origins of MUSO and relation to aging

Despite accumulating evidence for rhythmic infraslow oscillations, fundamental questions remain regarding their origin, reproducibility, and physiological significance. A key challenge is distinguishing MUSO from arrhythmic infraslow fluctuations below 0.2 Hz, which reflect the broadband 1/f activity [5,31]. The source of MUSO observed in noninvasive recordings remains unresolved — they could arise from neuronal dynamics, extraneuronal processes such as vasomotion, or even extracranial sources (e.g., skin vasomotion). Importantly, cerebral vasomotion exhibits rhythmicity within the same frequency range and produces near-sinusoidal oscillations remarkably similar to those of MUSO [32,33]. Because vasomotion influences microvascular tone and blood flow, it may also modulate blood–brain barrier (BBB) dynamics, which in turn can affect slow electrical potentials. Through this pathway, vascular rhythmicity could contribute to slow potential shifts such as MUSO detectable at the scalp [34–36], offering a plausible vascular-based framework for their generation. Furthermore, the substantial overlap between the frequency ranges of ISF and MUSO highlights the need for a mechanistic distinction between these signals. Studying healthy aging provides a unique opportunity to test hypotheses about the origin of MUSO, as age-related changes in vascular compliance, endothelial function, and BBB integrity [37–39] could amplify nonneuronal contributions relative to those of neuronal. Notably, while previous research on age-related neurophysiological changes has focused on faster neuronal oscillations above 1 Hz [40–45], the potential impact of aging on below 0.2 Hz electrophysiological signals remains largely unexplored.

In this study, we address these open questions by (1) identifying and validating MUSO in a large cohort via the open-access “Leipzig Study for Mind–Body–Emotion Interactions” (LEMON) [46] and characterizing their dependence on age, sex, and conditions (i.e., eyes-open/closed state) and (2) investigating the relationship between the MUSO and faster neuronal oscillations to assess its potential coupling with neuronal processes.

2. MATERIALS AND METHODS

2.1 Participants

We selected 175 participants across two age cohorts—younger (20–35 years) and older (55–75 years)—from an open resting-state EEG dataset collected at the Max Planck Institute for Human Cognitive and Brain Sciences [46]. While all individuals underwent rigorous medical and psychological screening before the study, we excluded 40 participants from the original dataset: 19 due to missing or inconsistent data (e.g., mismatched headers, varying sampling rates, or missing event info) and 21 due to poor signal quality (e.g., severe artifact bursts or extreme peak-to-peak deflections). The final sample comprised 113 younger adults (25.1±3.3 years, 38 females) and 62 older adults (67.5±4.83, 31 females). This research adhered to the

Declaration of Helsinki and was approved by the University of Leipzig ethics committee (reference number 154/13-ff).

2.2 Procedure

The recordings consisted of 16 minutes of resting-state EEG data, which were divided into 16 alternating 1-minute blocks of eyes-closed (EC) and eyes-open (EO) conditions (8 blocks each), beginning with an EC block. An acoustic cue before each block indicated the required state. The participants were instructed to stay awake and remain still throughout the recording; during the eyes-open blocks, they were further directed to fixate on a low-contrast cross.

2.3 EEG setup

EEGs were recorded via a Brain Products active cap system (ActiCAP, Brain Products GmbH, Germany) equipped with 62 channels. Of these, 61 active electrodes followed the international 10–20 configuration, whereas one channel was dedicated to tracking vertical eye movements from an infraorbital position below the right eye. We used FCz as the online reference point and fixed the ground to the sternum. Data acquisition was performed with a BrainAmp MR plus amplifier (Brain Products GmbH) with a 2500 Hz digitization rate, a 0.1 µV resolution, and a wide online bandpass filter spanning 0.015 Hz to 1 kHz.

2.4 EEG data analysis

EEG preprocessing. EEG preprocessing was conducted in MATLAB (MathWorks, Inc., Natick, MA, USA) via custom code integrated with EEGLAB v14.1.1b functions [47]. First, the continuous recordings were downsampled to 125 Hz. To prevent aliasing, we applied a low-pass filter with a 60 Hz cutoff (0.8 x Nyquist frequency) and a 12.5 Hz transition bandwidth (0.2 x Nyquist frequency). We then ran an independent component analysis (ICA) via the Infomax algorithm within EEGLAB to identify and strip out nonneural artifacts, including ocular blinks, eye movements, cardiac interference, and muscle activity.

Spatial Laplace filter. MUSO were shown to be particularly pronounced after spatial high-pass filtering [27]. To increase spatial specificity, we applied a spatial Laplacian filter, in which the mean of 4 adjacent electrodes was subtracted from the activity in a given electrode, resulting in 35 channels. By estimating how different the signal at one electrode is from the average of its neighboring electrodes, this method leads to spatially localized neuronal activity while reducing common activity [47]. Here, Laplace-filtered EEG data are referred to as EEG-L. In addition, for the later comparative analysis, we also used the original reference to FCz in which EEG data are referred to as EEG-FCz.

MUSO Measures* and *Time–Frequency Analysis. Spectral decomposition was performed with Welch's method via 60-second segments (*Hanning* window) with a 90% overlap. To quantify the relative periodic power (rPP) of the ~0.1 Hz oscillation, we applied a systematic method to characterize the spectral peak and separate it from the underlying 1/f noise. First, the frequency with the maximum value ($Fmax$) of the spectrum was identified by analyzing the derivative of the frequency spectrum and locating the zero-crossing point in the range of 0.065-0.17 Hz. If no positive rPP could be found in the MUSO range (which was the case for only ~ 2.4% of all channels and participants), a mean of the pooled channels was used instead. To

estimate the 1/f noise floor, a cubic interpolation was performed using four key points: the first point of the spectrum, $Fmax$ - 0.05 Hz, where Fmax was the frequency bin with the maximal power in 0.065-0.17 Hz, the dip point preceding the spectral peak ($Fdip$), and $Fmax$ + Δf (Δf=$Fmax$-$Fdip$ as the characteristic half-bandwidth of the oscillation). The peak frequency (Pf) was then determined as the maximum vertical deviation between the interpolated 1/f noise line and the original spectrum. The rPP was calculated as the ratio of the signal amplitude, defined as the difference between the spectral value at Pf and the noise value from the interpolated line at the same point to the noise amplitude. Supplementary Fig. 1 shows an example of an rPP calculation. This approach provides a robust measure of the prominence of the 0.1 Hz oscillation relative to the underlying noise. Additionally, the absolute periodic power (aPP) was calculated as the signal difference between the spectral (in dB) value at the peak frequency and the interpolated noise value.

Source analysis. We used forward volume conduction via the finite element method following the approach outlined by Huang et al. [48]. The geometry of the finite element method model was derived from the extended MNI/ICBM152 standard anatomy. The source space was restricted to the cortical surface and divided into 96 regions of interest (ROIs) using the Harvard–Oxford atlas [49]. To estimate the cortical electrical distribution from scalp EEG recordings, we employed eLORETA (exact low-resolution brain electromagnetic tomography) implemented in the M/EEG Toolbox of Hamburg (METH) [50,51]. The lead field matrix was computed for 2004 voxels distributed across the cortical surface. We subsequently applied singular value decomposition to the time series across voxels within each ROI to extract the component explaining the largest variance.

Statistical analysis of the effects of referencing, age group and sex. To investigate differences in rPP, aPP and Pf between the rereferencing methods (EEG-L and EEG-Fcz) and conditions (EO and EC), we conducted two-way repeated-measures analysis of variance (rm-ANOVA), with reference (EEG-L and EEG-Fcz) and conditions (EO and EC) as the independent variables and rPP, aPP, and Pf as the dependent variables. Linear regression analyses were conducted to examine the effects of age and sex on key spectral metrics, including rPP, aPP, and Pf. For each dependent variable, age was modeled as a continuous predictor, and sex was included as a categorical factor (with females as the reference group). Full model comparisons, including interaction terms, are provided in the Supplementary Material. Although the method we used removes the additive component of the 1/f background activity, its influence may still persist [15]. In particular, commonly used methods remove only the additive portion of the 1/f signal [16,52], leaving multiplicative components intact. As a result, residual aspects of the power-law structure may still bias spectral estimates, specifically by reducing rPP at higher peak frequencies. To address this potential confound, peak frequency was included as a covariate to isolate age and sex effects from frequency-related variability. Details regarding model improvements and statistical comparisons associated with the inclusion of peak frequency are provided in the Supplementary Material.

Regional MUSO Topography. To characterize the spatial distribution of MUSO activity, the 35 scalp electrodes (after Laplacian filtering) were grouped into six anatomical regions: frontal (AF3/AF4, F5–F6, F3/F4, F1/F2), frontocentral (FC5/FC3/FC4/FC6), central (C5–C6, C1–C4), centroparietal (CP5–CP6, CP1/CPz/CP2), parietal (P5–P6, P1/Pz/P2), and occipital (PO3/POz/PO4) regions. For each subject, the mean MUSO rPP was computed within each region, yielding six regional values.

Statistical analysis for MUSO Topography. Regional differences in MUSO rPP were assessed via repeated-measures ANOVA with region as a six-level within-subject factor. Post hoc pairwise comparisons (Bonferroni-corrected) were performed to determine which regions exhibited significantly higher or lower rPP. Potential influences of demographic factors on the spatial distribution of MUSO were tested with mixed-design ANOVAs that included region as a within-subject and sex (male/female) and age group (younger/older) as between-subject factors as well as region-by-sex and region-by-age group interactions.

Cross-frequency coupling between MUSO and fast EEG oscillations. *Phase–Amplitude Coupling*. To determine whether the phase of slow activity modulates the amplitude of faster EEG oscillations and to directly compare MUSO with a broader infraslow reference signal, we computed the modulation index [53] for two slow frequency ranges: (1) the subject-specific MUSO, defined as the individual peak frequency ± its bandwidth, that is, the pooled mean bandwidth across channels plus one standard deviation, and (2) the infraslow fluctuation range, defined as 0.02–0.1 Hz. The MUSO and ISF phase signals were extracted using a 2nd-order Butterworth filter with cutoff frequencies Fmax ± bandwidth for MUSO and 0.02–0.0.1 Hz range for ISF. Filtering was performed using Matlab's filtfilt function to avoid phase distortion. The analytic representation of each filtered signal was obtained via the Hilbert transform, and the instantaneous phase served as the slow-oscillatory reference for cross-frequency coupling analysis. Amplitude envelopes for the five neuronal frequency bands were subsequently extracted using standard bandpass filtering (2nd-order Butterworth filter) followed by the Hilbert transform. We used the phase signal of MUSO/ISF and the amplitude envelopes to compute the Modulation Index (MI). We implemented the following multistep workflow:

1) Phase Binning: The continuous phase signal was discretized into 18 equal intervals (bins) of 20° each, spanning from –180° to 180°.

2) Mean Amplitude Normalization: Within each phase bin j, the mean magnitude of the corresponding amplitude envelope was computed ($\underline{a_j}$). These values were then normalized across all *N* bins to generate an empirical probability distribution vector p:

$$p(j) = \frac{\underline{a_j}}{\sum_{k=1}^{N} \underline{a_k}} \quad (1)$$

where k is the running bin index and *N* = 18 represents the total number of phase bins.

3) Shannon Entropy Estimation: To evaluate the flatness of this normalized amplitude distribution, Shannon entropy (H) was calculated as:

$$H(p) = -\sum_{j=1}^{N} p(j) log p(j) \quad (2)$$

4) Kullback–Leibler (KL) Divergence: The disparity between the observed amplitude distribution (*X*) and a perfectly uniform distribution (U) was quantified via the KL distance:

$$KL(U,X) = logN - H(p) \quad (3)$$

where $logN$ acts as the theoretical entropy of a uniform distribution.

5) MI Scaling: Finally, the raw KL distance was normalized by dividing it by the uniform entropy ($logN$), yielding the bounded Modulation Index metric:

$$MI = \frac{KL(U,X)}{logN} \quad (4)$$

Statistical analysis for cross-frequency analysis. To detect the coupling between MUSO/ISF and faster oscillations robustly, we applied nonparametric permutation tests following the approach outlined by Maris and Oostenveld [54]. Additionally, a control analysis, as suggested by Aru et al. [55], was employed to validate the significance of phase–amplitude coupling values, ensuring robust measurements. Specifically, we generate 1000 surrogate datasets by permuting the phase time series. Surrogate data were created by dividing the original phase-MUSO (or phase-ISF) time series into 45-second segments and shuffling them in a random order. The null hypothesis assumes that the cross-frequency coupling values of the original data and the surrogate datasets are from the same distribution. We then computed the p value for the original signal pairs by comparing their coupling values against the distribution of surrogate values. To account for spatial dependencies induced by spatial Laplace filtering, we applied the FDR correction method of Benjamini & Hochberg [56], with a significance threshold of α = 0.05. FDR was applied for each subject separately such that 35 channels and 5 bands were combined.

Statistical analysis for cross-frequency coupling comparison between MUSO and ISF. To directly compare the strength of slow–fast coupling between MUSO and ISF, we used surrogate-normalized modulation indices (MIs). For each band, the MUSO and ISF MI values were compared across subjects via paired t tests (N = 175). The resulting five p values were corrected for multiple comparisons across bands via the Benjamini–Hochberg false discovery rate (FDR) procedure (q = 0.05).

3. RESULTS

3.1 MUSO occurrence and rPP

Our results show that MUSO exist in two distinct temporal forms: first, they can be present during the entire recording (16 min) with highly stable power over time, and second, or MUSO may appear only in certain segments varying between 1 minute and several minutes (Fig. 1: MUSO are present for the whole duration of the recordings; Fig. 2: MUSO are present in short segments). Further analysis indicated that 97.6% of the channels (pooled) presented positive rPP values (i.e., threshold rPP > 0, Laplace reference). In 11.6% of the channels, we detected a second peak, and in 0.4%, 3 peaks were indicated by rPP > 0 in the frequency range of 0.065–0.17 Hz. For the following analysis, if more than one peak was present, we focused on the peak with the largest rPP. However, there was a considerable decrease in the number of channels as the rPP threshold increased (Fig. 3).

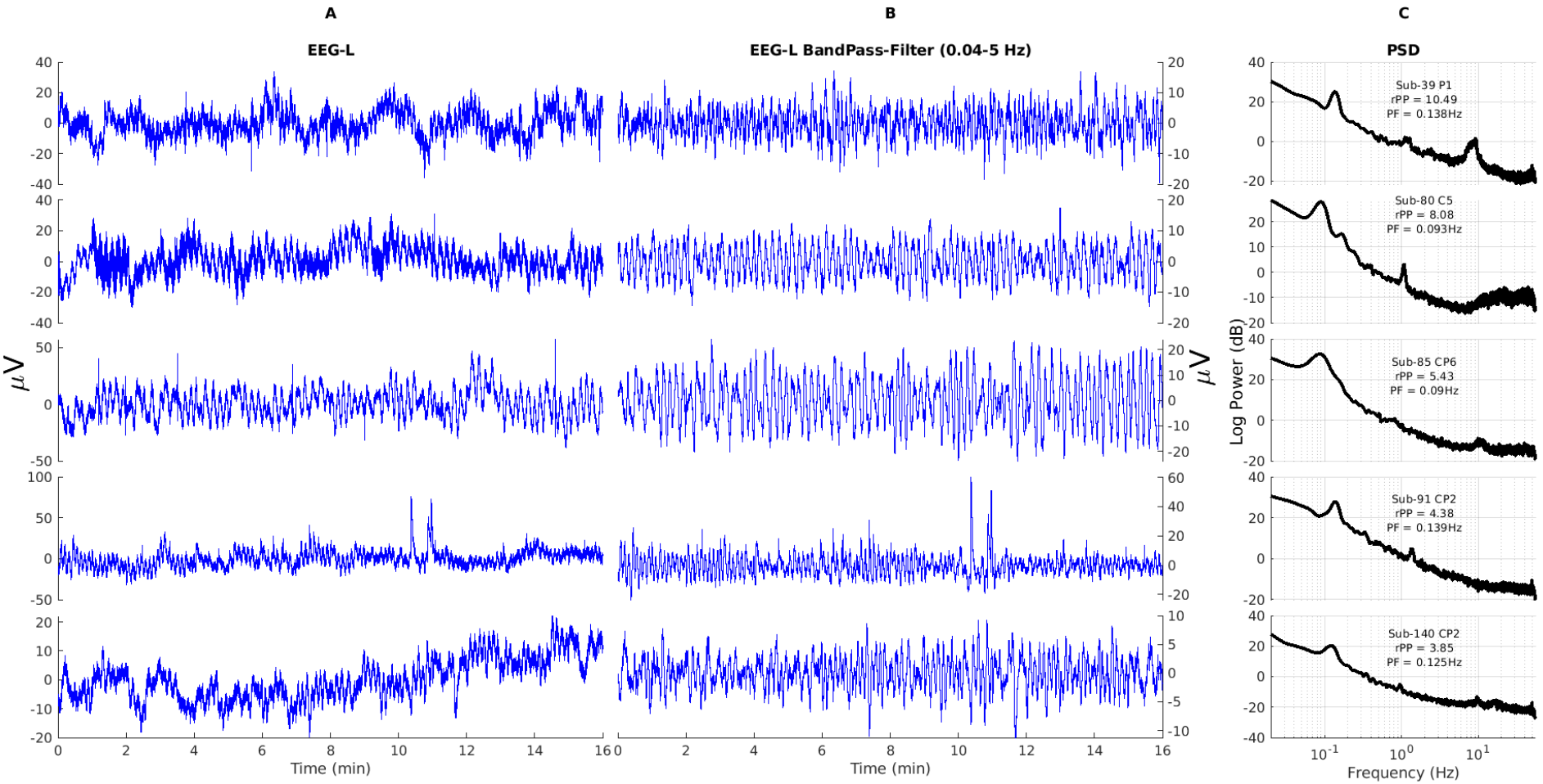
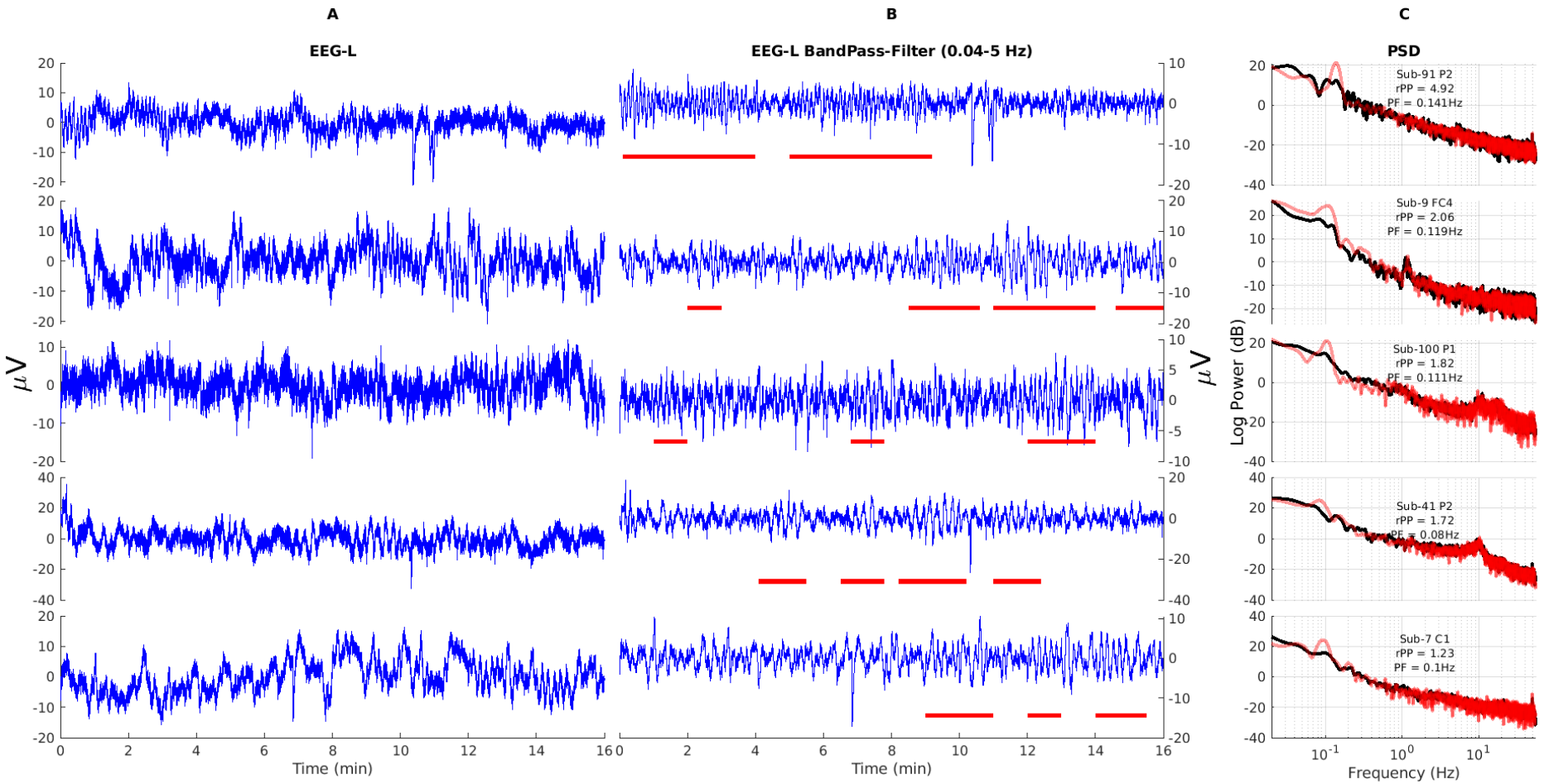


Figure 1. Representative 16-minute EEG recordings from five participants exhibiting persistent MUSO. (A) Broadband (0.015–125 Hz) Laplace-filtered EEG (EEG-L) signals showing pronounced oscillations across the entire 16-minute recording, sorted by relative periodic power (rPP). **(B)** Bandpass-filtered (0.04–5 Hz) EEG-L signals. This filtering, however, is still sufficiently broad not to produce MUSO by the filtering itself. **(C)** Power spectral density (PSD) of the EEG-L signals for each participant, demonstrating distinct monochromatic peaks near ~0.1 Hz. **C**. The graphs show the power spectral density (PSD) of the EEG-L. Monochromatic peaks at approximately 0.1 Hz can be clearly observed. Each EEG recording is selected from different subjects (indicated in each spectrum).

Figure 2. Representative 16-minute EEG recordings from five participants exhibiting transient Monochromatic Ultra-Slow Oscillations (MUSO). (A) Broadband (0.015–125 Hz) Laplace-filtered EEG (EEG-L) signals showing transient episodes of MUSO. **(B)** Bandpass-filtered (0.04–5 Hz) EEG-L signals highlighting segment-specific oscillatory activity. **(C)** Power spectral density



(PSD) of the EEG-L signals. Spectral estimations corresponding to the highlighted MUSO segments (red) show prominent monochromatic peaks compared to non-MUSO segments (black). Data are shown for representative channels from five distinct subjects.

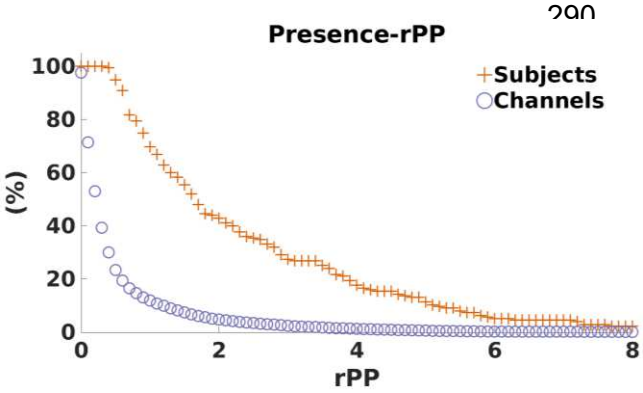


Figure 3. Percentage of MUSO occurrence for participants and channels related to relative periodic power (rPP). The circles represent the percentage of channels (pooled) above the given level (x-axis). The crosses represent the percentage of participants who have at least one channel above the given level of rPP. Participants who had at least one channel above the corresponding rPP level on the x-axis were included in the percentage count at the subject level.

3.2 Effects of the spatial Laplace (-L) filter and eyes-open (EO) and eyes-closed (EC) conditions on the MUSO parameters

For these analyses, we first averaged the spectra across all electrodes. Two-way rm-ANOVA with factors condition (EO, EC) and reference (EEG-L, EEG-Fcz) revealed a significant main effect of reference on the rPP ($F(1,174) = 22.152$, $p = 5.1 \times 10^{-6}$), and post hoc analysis further indicated that spatial Laplace filter referencing provided a stronger rPP (Fig. 4A). In addition, we found a significant main effect of reference on aPP ($F(1,174) = 11.01$, $p = 0.04$), with post hoc analysis revealing that EEG-L has a greater aPP than does EEG-FCz (Fig. 4B). We also examined the influence of rereferencing on the peak frequency, which is an important parameter for estimating the rPP. There was no main effect of electrode referencing on peak frequency (Fig. 4C). As there was no significant difference between eyes open/eyes closed conditions for any of the measures (rPP, Pf, aPP), the data were concatenated (resulting in 16 min of recording) to obtain more reliable estimates for further comparisons. Crucially, owing to the stronger rPP of MUSO achieved with the Laplace filter than with the EEG-FCz reference, therefore we used EEG-L for subsequent statistical analyses.

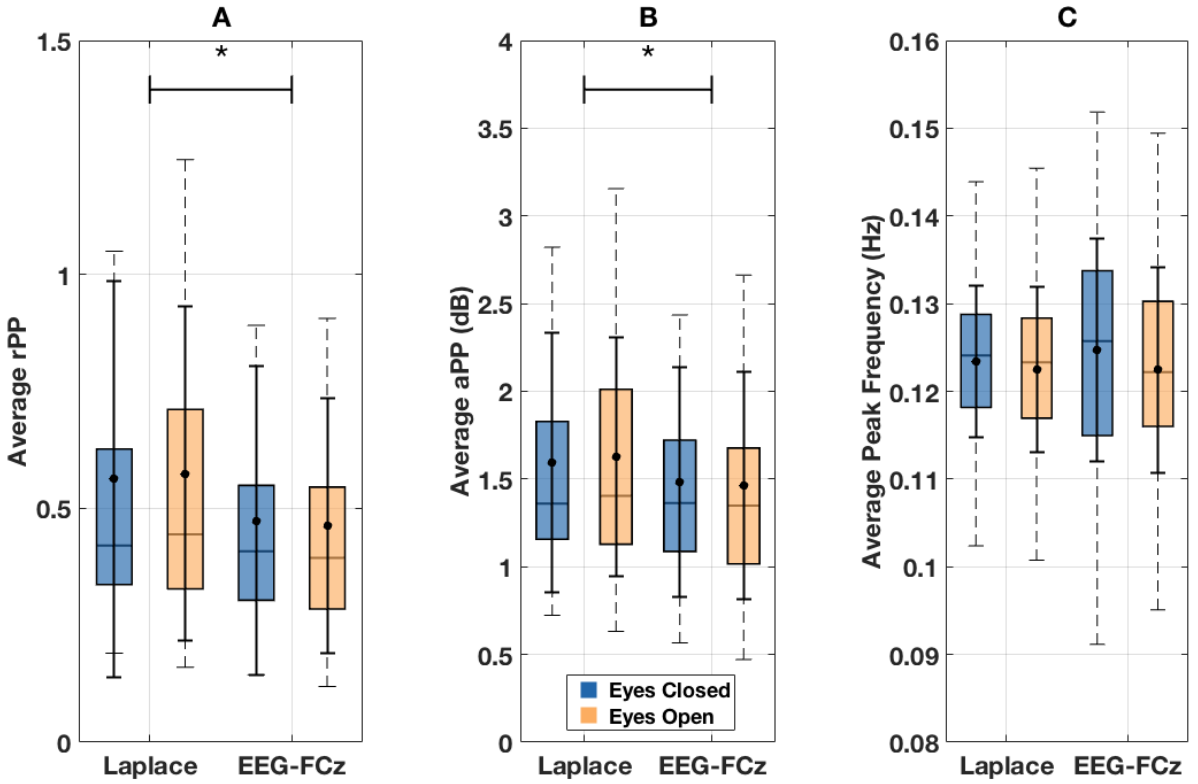


Figure 4. Effects of the conditions and reference scheme on the MUSO metrics. Boxplots illustrate the distribution of subjectwise average values for three MUSO metrics: **(A)** relative periodic power (rPP), **(B)** absolute periodic power (aPP), and **(C)** peak frequency (Pf). For each metric, the data are shown separately for the Laplace-referenced and FCz-referenced EEG (grouped on the x-axis) and for the eyes-closed (blue) and eyes-open (yellow) resting-state conditions. Boxes indicate the interquartile range (IQR), with the median marked by the central horizontal line; whiskers extend to the most extreme nonoutlier values. The black circles denote the means, with vertical error bars indicating ±1 standard deviation across subjects. All values represent within-subject averages across channels (for EEG-FCz data restricted to the subset mapped to Laplace channels). The horizontal brackets and asterisks indicate significant differences between reference schemes ($p < 0.05$).

3.3. Topography of MUSO

The grand average across all the subjects revealed that the rPP and aPP of MUSO was most prominent in the parietal, occipital, and temporal areas, as shown in Fig. 5A. We further performed source modeling via eLORETA for rPP and aPP across all the subjects (N = 175). Confirming the results from the sensor space, the sources for MUSO (in the grand average) were most prominently located in parietal areas (Fig. 5C). In addition, the repeated-measures ANOVA revealed a significant effect of region on MUSO rPP ($F(5,870) = 10.75$, $p=4.83\times10^{-10}$), indicating robust topographic differences. Post hoc comparisons revealed that the centroparietal, parietal and central regions presented significantly greater rPP than did the frontal and frontocentral regions (all $p < 0.01$) (Supplementary Figure 2).

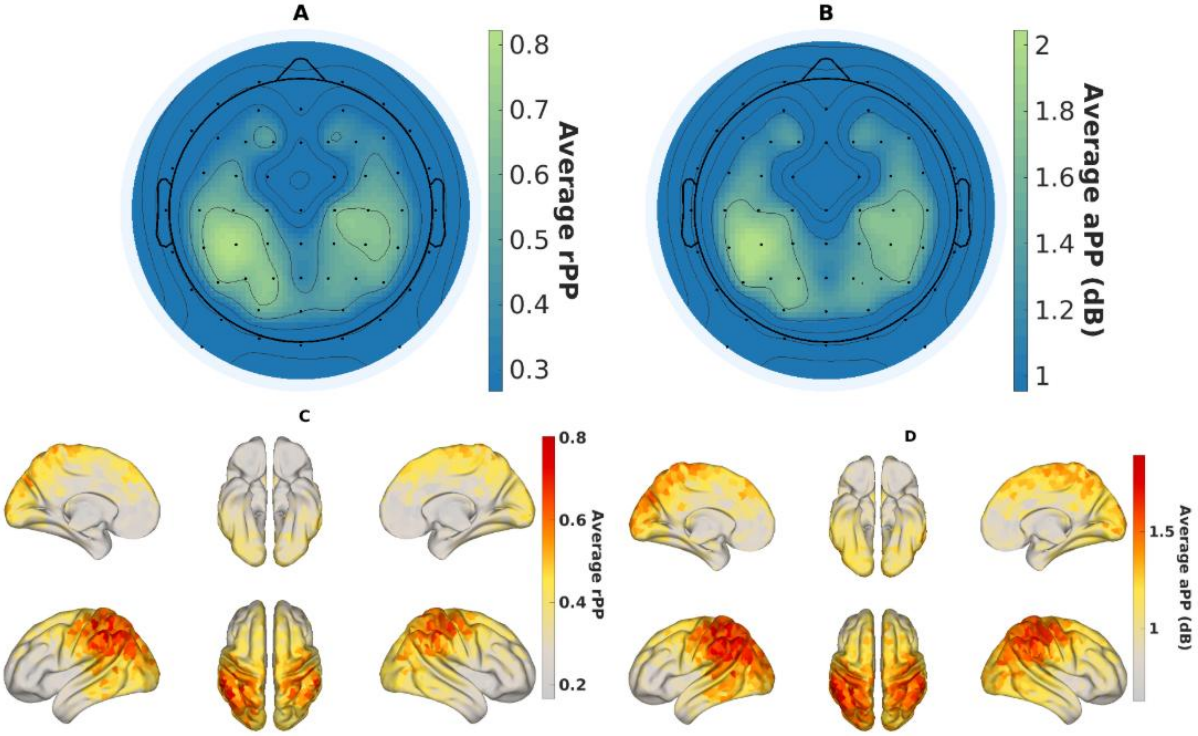


Figure 5. Topography of MUSO. (A) Heatmaps presented as the average relative periodic power (rPP) across all participants. The parietal, occipital, and temporal areas presented the highest rPP values, suggesting that these regions are particularly active in generating MUSO. **(B)** The average absolute period power (aPP) of MUSO. Similar to the rPP heatmap, the areas with the highest aPP coincided with those with the highest rPP, supporting the idea that the parietal, occipital, and temporal regions are key loci for MUSO activity. (**C)** Cortical maps of average rPP from source space analysis reveal that the sources of MUSO are predominantly located in the parietal areas of the left hemisphere. (**D)** Cortical maps of the average aPP show that the aPP is distributed similarly to the rPP, such that it is located in the parietal areas.

3.4 Age and sex differences in the MUSO (sensor space EEG-L)

A linear regression model including age (as a continuous variable) and sex as predictors revealed significant effects of both variables on relative periodic power (rPP). Older age was

associated with reduced rPP (β = -0.0051, p = 0.0019), and males presented lower rPP than females did (β = -0.26, p = .00018). Similarly, both age (β = -0.0099, p = .001) and sex (β = –0.50, $p = 8.2\text{x}10^{-5}$) significantly predicted absolute periodic power (aPP), with males and older individuals showing lower values. We also observed that the peak frequency was lower in females and in younger individuals. Older subjects had a higher peak frequency (β = 0.00012, p = .0021). In addition, males had a greater peak frequency than females did (β = 0.0061, p = .00022) (Fig. 6C). To account for potential residual power-law influences (where a 1/f shape can lead to lower peak frequencies being associated with higher values), we conducted a separate analysis including peak frequency as a covariate. When peak frequency was added to the model predicting rPP, larger peak frequencies were associated with lower rPP (β = –17.3, $p = 2.1\text{x}10^{-8}$), yet age (β = –0.003, p = .048) and sex effects (β = –0.16, p = .017) remained significant with the same directionality as in the former model. Likewise, in the aPP model, peak frequency again showed a strong negative association with rPP (β = –31.4, $p = 1.9\text{x}10^{-8}$), yet age (β = –0.0061, p = .029) and sex (β = –0.31, p = .0097) continued to have significant effects. These additional models suggest that age and sex remain significant predictors even when their shared variances with peak frequency, potentially reflecting the residual influence from the 1/f, are taken into account by the model. Interaction effects between age and sex were initially tested but found to provide limited explanatory benefit; therefore, only main-effect models are reported in the main text.

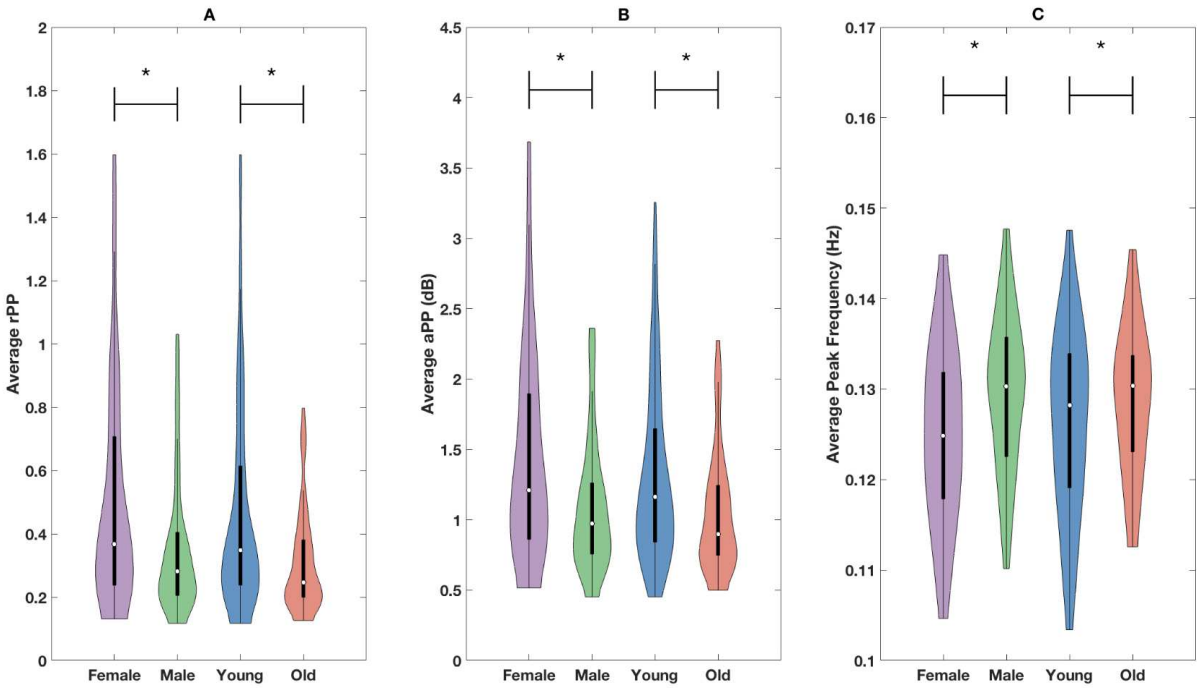


Figure 6. Age and sex MUSO differences. (A) Average relative periodic power (rPP) represents the average rPP of MUSO across different age groups and sex groups. The analysis revealed significant main effects of age group and sex on rPP, with younger participants exhibiting higher rPP than older participants and female participants showing higher rPP than male participants did, suggesting that age and sex are important factors for the detectability of MUSO in EEG recordings. **(B)** Average aPP displays violin plots of the average aPP of MUSO across age and sex groups. Similar to the peak frequency, the average aPP was calculated by including only the channels exhibiting rPP > 0 in the frequency range of interest (0.065--0.17 Hz). The plots reveal that younger participants have higher aPP than older participants do. **(C)** Average peak frequency featuring the peak frequency of MUSO across the same age and sex groups. The average peak frequency was calculated by including only the channels that exhibited rPP > 0 within the frequency range of interest (0.065–0.17 Hz). The vertical range highlighted with a black bar represents the interquartile range (25%-75%). The median is highlighted with a white dot.

3.5 Age and sex differences in topography of the MUSO rPP (sensor space EEG-L)

A mixed ANOVA including sex as a between-subject factor revealed that the region × sex interaction was not significant ($F(5,865) = 1.80$, $p = 0.11$) for rPP, indicating that the topographic pattern was comparable across sexes. Similarly, age showed a nonsignificant region × age interaction effect ($F(5,865) = 0.36$, $p = 0.88$). Thus, neither sex nor age altered the spatial distribution of MUSO activity, and posterior–central enhancement was consistently observed across all groups (Fig. 7).

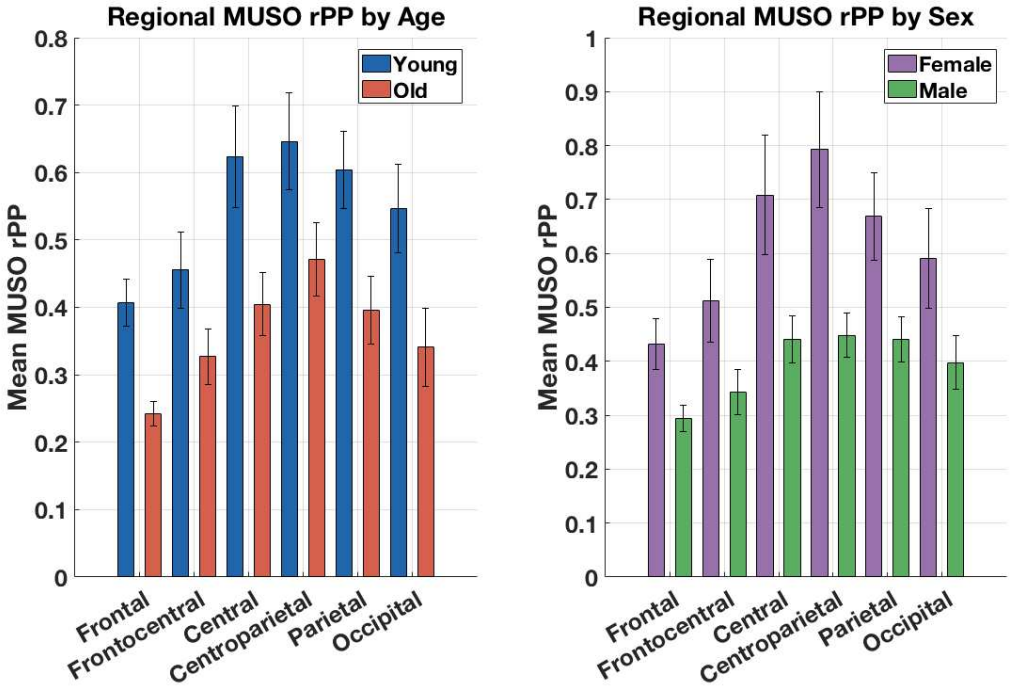


Figure 7. Age and sex differences in regional MUSO rPP. Mean relative peak power (rPP) of the monochromatic ultraslow oscillation (MUSO; ~0.1 Hz) plotted across six canonical scalp regions, separated by age group (left) and sex (right). Compared with older adults, young participants presented greater MUSO rPP, particularly over the centroparietal and parietal regions, indicating an age-related decline in ultraslow oscillatory power. Compared with males, females presented greater MUSO rPP across all regions, with the largest differences observed over central and centroparietal sites. The error bars denote the standard error of the mean (SEM). Together, these results suggest that both age and sex modulate the amplitude of slow cortical oscillations across the entire cortex.

3.6 Relationships between the MUSO and genuine neuronal oscillations

We conducted cross-frequency coupling analyses to investigate the relationships between the MUSO and neuronal oscillations in conventional delta (1–4 Hz), theta (4–7 Hz), alpha (7–15 Hz), beta (15–25 Hz) and low gamma (25–45 Hz) bands via phase–amplitude coupling. Across subjects, MUSO exhibited extremely sparse significant phase–amplitude coupling with conventional neuronal frequency bands. Before correction, 8.1% of the MUSO channel × band combinations exceeded the surrogate-based significance threshold, and this proportion was reduced to 0.4% after controlling for multiple comparisons via the FDR correction. Thus, only a very small fraction of the MUSO-derived coupling estimates reached statistical significance. For ISF, the same analysis yielded a similar coupling incidence. Prior to FDR correction, 8.2% of the ISF channel × band pairs were significant, and only 0.5% remained significant after FDR correction. Importantly, this low incidence of absolute significance likely reflects the highly conservative nature of our single-channel correction approach, which substantially reduces the statistical power for detecting subtle, localized effects. An example from a single subject

and channel is shown in Supplementary Figure 4, where the empirical phase–amplitude curve is displayed together with its surrogate distribution. While individual traces occasionally exhibited mild deviations from surrogate fluctuations, these effects were generally small and did not extend systematically across channels or subjects. To evaluate whether infraslow fluctuations and MUSO exhibit distinct baseline relationships with faster neuronal activity, we compared band-specific modulation index (MI) values averaged across channels for delta, theta, alpha, beta, and gamma amplitude envelopes. Across all frequency bands, ISF consistently presented higher baseline MI values than MUSO did, even though neither reached robust absolute significance. As illustrated in Supplementary Figure 5, the MI values were greater for ISF than for MUSO in each band, with nonoverlapping or minimally overlapping standard error margins, indicating robust differences. These observations were confirmed statistically using paired *t* tests across participants (n = 175), with multiple-comparison correction across the five frequency bands. As summarized in Supplementary Table 2, all comparisons reached high statistical significance after false discovery rate (FDR) correction (all $q < 10^{-19}$), with large standardized effect sizes (Cohen's *dz* values ranging from 0.79-1.41).

4. DISCUSSION

In this study, we investigated the characteristics of MUSO by analyzing resting-state EEG data to better understand the mechanisms underlying these oscillations. We observed MUSO in many participants, where MUSO appeared as nearly sinusoidal oscillations in the time domain and as a prominent peak at approximately 0.1 Hz in the frequency domain. Compared with the FCz reference, spatial Laplace filtering significantly increased the relative periodic power (rPP) and absolute periodic power (aPP), with no effect on the peak frequency. Spatially, rPP-MUSO were most pronounced in the occipito-parietal areas in both the sensor space and the source space. Age and sex also influenced MUSO characteristics: younger participants and females presented higher rPP and aPP than older and male participants did. Importantly, we found no effect of eyes-open (EO) or eyes-closed (EC) conditions on any of the parameters, including rPP, aPP, or Pf. Finally, we found no evidence of cross-frequency coupling between MUSO and faster neural oscillations.

4.1 MUSO characteristics

Our main finding is a confirmation of MUSO in an independent large dataset of participants, thus building on earlier observations from a study with only nine participants [27]. We also identified differences in the MUSO parameters depending on the rereferencing schemes. The spatial Laplace filter produced higher rPP and aPP values, which aligns with earlier findings from Nikulin et al. [27] and suggests that MUSO may originate from focal sources. MUSO were present in two distinct patterns across participants: some exhibited stable oscillations that persisted throughout the entire recording, whereas others displayed intermittent oscillations appearing only in a few segments. These patterns were observed consistently, irrespective of behavioral conditions such as eyes opening or closing.

4.2 Insensitivity to eyes-open eyes-closed conditions

An early study [24] reported that various stimuli, including tactile and visual inputs, as well as mental activities such as arithmetic calculations, meditation, and memory recollections, failed

to induce rhythmic infraslow activity below 0.16 Hz. Consistent with these findings, our study demonstrated that the MUSO were not sensitive to eyes-open or eyes-closed conditions in any brain region, including the occipitoparietal areas, which are typically responsive to significant changes in visual input [57,58]. Given that the MUSO are predominantly observed in occipitoparietal areas, this lack of sensitivity to visual sensory manipulation suggests that the MUSO may not be associated with neuronal processes traditionally associated with visual input (e.g., eyes closing as a strong modulator). Moreover, the lack of cross-frequency coupling between the MUSO phase and alpha-band amplitude, an oscillatory feature well known to vary with eyes-open and eyes-closed states, further supports the notion that the MUSO likely reflects extraneuronal sources (see below).

4.3 MUSO and their relation to conventional neuronal oscillations

Some previous EEG studies have demonstrated a coupling of the phase of infraslow fluctuations with the amplitude of higher-frequency neuronal oscillations [5,7,12,29]. Although the specific ISF frequency range varied across studies (typically 0.01–0.1 Hz or 0.02–0.2 Hz), these findings suggest that a certain portion of infraslow activity is coupled to neuronal oscillations in higher-frequency ranges during sensory stimulation [5], sleep [7], rest in postanoxic coma patients [29], and during resting-state transcranial magnetic stimulation in healthy subjects [12]. Furthermore, invasive cortical recordings in monkeys [59] and humans [60,61] demonstrated that oscillations spanning from delta (1–4 Hz) to high-gamma (100–150 Hz) frequency bands exhibit pronounced amplitude modulation in the infraslow range. Importantly, many of the abovementioned studies relied on a small number of electrodes or group-level statistical approaches, and several examined non–resting-state conditions where neuronal coupling is known to increase. In contrast, our analyses were performed at rest, across a 35-channel Laplace-filtered montage, and with conservative statistics at the single-channel level. Under these conditions, MUSO and ISF exhibited only modest coupling, considerably weaker than what has been reported under task [5] or sleep paradigms [7]. Despite the very low occurrence of coupling between MUSO/ISF and faster signals in our dataset, ISF displayed a systematic increase in the normalized modulation index across the theta–gamma bands compared with MUSO. Taken together, our findings demonstrate that while both infraslow phenomena exhibit minimal absolute coupling to faster rhythms at rest, they display highly consistent numeric separation in their baseline modulation index (MI) values. This clear statistical separation suggests that MUSO and ISF arise from distinct underlying processes, with MUSO reflecting a mechanism that is even more thoroughly isolated from ongoing synaptic networks than broad-band ISF.

4.4 Linking vasomotion and Blood–Brain Barrier electrochemistry to MUSO generation

Nikulin et al. [27] reported that MUSO were coherent with arterial blood pressure and fNIRS signals. They concluded that MUSO might reflect cerebral vasomotion. Further evidence supporting a nonneuronal contribution to MUSO comes from early observations of the near-DC potential of several millivolts between cerebrospinal fluid and blood, arising from the partial permeability of plasma solutes across the blood–brain barrier (BBB) [34,35]. Voipio et al. [36] proposed that the BBB functions as a voltage source, generating a volume current through distributed resistance. In line with Nikulin et al. [27], we believe that this voltage source is not mechanically static but is dynamically influenced by rhythmic vascular activity, particularly

vasomotion—the slow, periodic dilation and constriction of blood vessels. Vasomotion imposes oscillatory shear stress on endothelial cells, and shear stress produced by microvascular blood flow serves as a fundamental signal that governs vasomotor responses through the stimulation of endothelial mechanotransduction pathways [62]. The activation of these pathways can modulate BBB permeability and ion transport [63,64], leading to fluctuations in ionic gradients and transendothelial resistance. Through these mechanisms, vasomotion-driven shear forces may periodically modulate the near-DC potential across the BBB, thereby linking vascular dynamics directly to the slow electrical activity observed in the brain. Our findings support this interpretation and align with previous evidence of ~0.1 Hz coherence between hemodynamic signals and EEG signals [27], suggesting that MUSO may emerge from the dynamic interplay between vascular activity, endothelial mechanotransduction, and the electrochemical properties of the BBB. This mechanism of modulating the voltage gradient across the BBB requires periodic mechanical modulation at approximately 0.1 Hz. In fact, several previous studies have reported spontaneous slow hemodynamic oscillations in oxy-deoxyhemoglobin signals, which share frequencies similar to those of MUSO [32,33] and exhibit strikingly similar spectral properties. These oscillations have been linked to local vasomotor processes and are characterized by nonsystemic, highly localized patterns. Notably, spontaneous slow hemodynamic oscillations and MUSO both occur within the same frequency range (0.04–0.18 Hz), suggesting that MUSO could represent the electrical counterpart of local vasomotion-related BBB potential changes described above. This alignment further strengthens the earlier hypothesis that the MUSO may be driven primarily by vascular mechanisms [27], particularly cerebral vasomotion, rather than neural activity alone. Further evidence for nonneuronal contributions comes from studies investigating neurovascular coupling. For example, research assessing the visual thalamus of cats revealed spontaneous slow sinusoidal hemodynamic oscillations at 0.14 Hz, which disrupted the relationship between local neuronal activity and blood flow [65]. Similarly, laser Doppler spectroscopy in rats revealed strong sinusoidal hemodynamic fluctuations at approximately 0.1 Hz following sharp changes in blood pressure, which diminished the correlation between neuronal and hemodynamic signals during isoflurane-induced neuronal bursting [66]. Additionally, Mitra et al. [67] demonstrated in mice that infraslow oscillations (<0.1 Hz) exhibit dynamics distinct from those of higher-frequency oscillations, suggesting that they should be considered separate physiological processes. These findings align with our results, indicating a lack of coupling between the MUSO and faster neuronal oscillations.

4.6 Effects of age and sex on the MUSO

With respect to slow oscillations <0.2 Hz, a recent study with concurrent fNIRS and EEG measurements revealed that elderly subjects exhibit reduced coherence between EEG and fNIRS signals in the 0.052–0.145 Hz range compared with younger participants [14]. The authors suggest that this association stems from vascular changes that occur with healthy aging. In line with these findings, our study also revealed pronounced age-related differences in MUSO-rPP and aPP, with older participants exhibiting lower rPP and aPP. This reduction may be attributed to age-related vascular changes, such as diminished vessel elasticity [37], which could lead to weaker vasomotor activity and reduced variations in BBB potential, as explained above. Research has shown that age significantly impacts BBB permeability, with younger individuals having lower permeability than older adults do [39], and that aging is associated with ion imbalances, leakage of plasma proteins, and other consequences of BBB

breakdown [38]. These changes likely reduce the electromotive force across the BBB and consequently may contribute to the lower MUSO rPP and aPP observed in older adults.

Similarly, sex had a notable influence on MUSO, with females displaying higher MUSO rPP and aPP values than males. The observed sex differences in MUSO characteristics may be attributed to variations in BBB permeability, as females have been shown to exhibit lower BBB permeability [68,69]. Additionally, shear stress has been reported to be greater in adult females [70], and vasodilation is more robust in female cerebral arteries than in male cerebral arteries in vivo [71]. These factors may contribute to the stronger MUSO observed in female participants. Another factor potentially influencing MUSO rPP/aPP alterations could be arterial compliance, which is generally greater in females [72] and younger [73] individuals than in males and older individuals. Consequently, lower vascular compliance can reduce variations in BBB potential due to weak vasomotion, resulting in lower MUSO-rPP. These findings are consistent with the hypothesis that the MUSO may represent the electrical counterpart of slow sinusoidal hemodynamic oscillations, further linking MUSO characteristics to vascular and endothelial factors that modulate BBB function such that lower permeability results in greater potential differences at the BBB. Finally, when we consider the peak frequency of MUSO, we find it to be on average approximately 0.12 Hz with a standard deviation of 0.023 Hz, indicating that most peak MUSO frequencies (i.e., 69% of the channels) are above 0.1 Hz. This observation is crucial, as it highlights a potential oversight in some infraslow EEG studies that fail to account for frequencies above 0.1 Hz, leading to either disregard or partial inclusion of MUSO and potentially resulting in inconsistent results. Therefore, slow cortical and scalp potentials may also involve nonneuronal mechanisms. Specifically, they could be influenced by the electrical potential difference across the BBB.

4.7 Potential clinical implications

EEG-based monitoring of the MUSO is clinically relevant, as alterations in the frequency and amplitude of these oscillations may serve as sensitive, noninvasive biomarkers for neurovascular and metabolic diseases. In stroke, disruptions in both neurovascular coupling and BBB integrity are central pathological features [74], and MUSO characteristics may provide early indicators of ischemic damage for timely intervention. Similarly, in migraine, cortical spreading depolarizations drive transient BBB permeability and localized hemodynamic changes that align with MUSO's frequency range [75], suggesting applications in diagnosis. Metabolic disorders such as type 2 diabetes are associated with impaired vasomotion and increased BBB permeability, which may alter MUSO [76]. In aging and neurodegenerative disorders such as Alzheimer's disease and Parkinson's disease, reduced vasomotion and BBB dysfunction accelerate disease progression [77,78], and the MUSO could capture these changes noninvasively. Thus, EEG MUSO analysis may enable targeted monitoring and assessment of disease states and therapeutic responses across diverse clinical contexts.

4.8 Limitations

A key limitation of this study is the absence of simultaneous intraoperative multispectral optical intrinsic signal imaging (MS-OISI) and electrocorticography (ECoG) recordings, which would have allowed us to directly assess whether the MUSO originates from local cortical activity or extracranial sources. While scalp EEG is well suited for capturing ultraslow dynamics, the lack of ground truth data from invasive recordings limits our ability to definitively attribute these

oscillations to vascular or neuronal processes. Additionally, in the LEMON dataset, there were no concurrent peripheral physiological measurements, such as peripheral vasomotion, simultaneous blood pressure oscillations, or autonomic rhythms (i.e., heart rate), which might have provided valuable insight into the potential systemic contributions to the MUSO. Future work combining EEG with multimodal recordings, including ECoG, peripheral sensors, or even MS-OISI, would help clarify the origin and mechanism of MUSO.

5. CONCLUSION

This study further characterizes MUSO as a robust and distinct feature of human EEG, with clear topographical patterns and significant modulation by age and sex. Unlike faster neuronal oscillations, the MUSO is not sensitive to the behavioral state or clear cross-frequency coupling, suggesting that it might reflect extraneuronal processes tied to cerebral vasomotion and blood–brain barrier dynamics. These findings underscore the importance of considering nonneuronal sources in EEG research and suggest that MUSO could serve as a promising biomarker for neurovascular function. Future work integrating multimodal imaging and clinical studies will be critical to fully realize the diagnostic and translational potential of MUSO in neurological disorders.

Additional information

Competing Interests and Funding

The authors have no relevant financial or non-financial interests to disclose. This research received no specific grant from any funding agency in the public, commercial, or not-for-profit sectors.

Data Availability

The raw EEG and demographic data analyzed during the current study are publicly available in the Leipzig Study for Mind-Body-Emotion Interactions (LEMON) repository (available via https://ftp.gwdg.de/pub/misc/MPI-Leipzig_Mind-Brain-Body-LEMON/). The processed variables and intermediate data generated during this study have been deposited in Zenodo and are publicly accessible under DOI: [https://doi.org/10.5281/zenodo.21669560].

Code Availability

All custom MATLAB scripts, functions, and pipeline code used to process the data, perform statistical analyses, and generate the figures in this manuscript are permanently archived on Zenodo under DOI: [https://doi.org/10.5281/zenodo.21669560]. The code relies on MATLAB (v2023a) and open-source toolboxes including EEGLAB, METH (meth_2019_04), and local plotting utilities as described in the repository README.

References

1. Buzsaki, G. & Draguhn, A. Neuronal oscillations in cortical networks. *Science* **304**, 1926–1929 (2004).
2. Palva, J. M. & Palva, S. Infra-slow fluctuations in electrophysiological recordings, blood-oxygenation-level-dependent signals, and psychophysical time series. *Neuroimage* **62**, 2201–2211 (2012).
3. Watson, B. O. Cognitive and physiologic impacts of the infraslow oscillation. *Front. Syst. Neurosci.* **12**, 44 (2018).
4. Kropotov, J. D. The enigma of infra-slow fluctuations in the human EEG. *Front. Hum. Neurosci.* **16**, 928410 (2022).
5. Monto, S., Palva, S., Voipio, J. & Palva, J. M. Very slow EEG fluctuations predict the dynamics of stimulus detection and oscillation amplitudes in humans. *J. Neurosci.* **28**, 8268–8272 (2008).
6. Hiltunen, T. *et al.* Infra-slow EEG fluctuations are correlated with resting-state network dynamics in fMRI. *J. Neurosci.* **34**, 356–362 (2014).
7. Vanhatalo, S. *et al.* Infraslow oscillations modulate excitability and interictal epileptic activity in the human cortex during sleep. *Proc. Natl. Acad. Sci.* **101**, 5053–5057 (2004).
8. Hughes, S. W., Lőrincz, M. L., Parri, H. R. & Crunelli, V. Infraslow (< 0.1 Hz) oscillations in thalamic relay nuclei: Basic mechanisms and significance to health and disease states. *Prog. Brain Res.* **193**, 145–162 (2011).
9. Orlowska-Feuer, P. *et al.* Infra-slow modulation of fast beta/gamma oscillations in the mouse visual system. *J. Physiol.* **599**, 1631–1650 (2021).
10. Picchioni, D. *et al. Infraslow EEG Oscillations Organize Large-Scale Cortical–Subcortical Interactions during Sleep: A Combined EEG/fMRI Study*. (Brain Research, 2011).
11. Helps, S., James, C., Debener, S., Karl, A. & Sonuga-Barke, E. J. S. Very low frequency EEG oscillations and the resting brain in young adults: A preliminary study of

localisation, stability and association with symptoms of inattention. *J. Neural Transm.* **115**, 279–285 (2008).

12. Goede, A. A. & Putten, M. J. Infraslow activity as a potential modulator of corticomotor excitability. *J. Neurophysiol.* **122**, 325–335 (2019).

13. Hashimoto, H. *et al.* Phase-amplitude coupling between infraslow and high-frequency activities well discriminates between the preictal and interictal states. *Sci. Rep.* **11**, 17405 (2021).

14. Bjerkan, J. *et al.* Aging affects the phase coherence between spontaneous oscillations in brain oxygenation and neural activity. *Brain Res. Bull.* **201**, 110704 (2023).

15. Gerster, M. *et al.* Separating neural oscillations from aperiodic 1/f activity: Challenges and recommendations. *Neuroinformatics* **20**, 991–1012 (2022).

16. Donoghue, T. *et al.* Parameterizing neural power spectra into periodic and aperiodic components. *Nat. Neurosci.* **23**, 1655–1665 (2020).

17. He, B. J., Zempel, J. M., Snyder, A. Z. & Raichle, M. E. The temporal structures and functional significance of scale-free brain activity. *Neuron* **66**, 353–369 (2010).

18. Palva, S. & Palva, J. M. Roles of brain criticality and multiscale oscillations in temporal predictions for sensorimotor processing. *Trends Neurosci.* **41**, 729–743 (2018).

19. Blythe, D. A. & Nikulin, V. V. Long-range temporal correlations in neural narrowband time-series arise due to critical dynamics. *PloS One* **12**, 0175628 (2017).

20. Voytek, B. *et al.* Age-related changes in 1/f neural electrophysiological noise. *J. Neurosci.* **35**, 13257–13265 (2015).

21. Schaworonkow, N. & Voytek, B. Longitudinal changes in aperiodic and periodic activity in electrophysiological recordings in the first seven months of life. *Dev. Cogn. Neurosci.* **47**, 100895 (2021).

22. Aladjalova, N. A. Infra-slow rhythmic oscillations of the steady potential of the cerebral cortex. *Nature* **179**, 957–959 (1957).

23. Aladjalova, N. A. *Slow Electrical Processes in the Brain*. (Elsevier, 1964).

24. Girton, D. G., Benson, K. L. & Kamiya, J. Observation of very slow potential oscillations in human scalp recordings. *Electroencephalogr. Clin. Neurophysiol.* **35**, 561–568 (1973).
25. Trimmel, M., Mikowitsch, A., Groll-Knapp, E. & Haider, M. Occurrence of infraslow potential oscillations in relation to task, ability to concentrate and intelligence. *Int. J. Psychophysiol.* **9**, 167–170 (1990).
26. Okun, M., Steinmetz, N. A., Lak, A., Dervinis, M. & Harris, K. D. Distinct structure of cortical population activity on fast and infraslow timescales. *Cereb. Cortex* **29**, 2196–2210 (2019).
27. Nikulin, V. V. *et al.* Monochromatic ultra-slow (0.1 Hz) oscillations in the human electroencephalogram and their relation to hemodynamics. *Neuroimage* **97**, 71–80 (2014).
28. Marshall, L., Mölle, M., Fehm, H. L. & Born, J. Scalp recorded direct current brain potentials during human sleep. *Eur. J. Neurosci.* **10**, 1167–1178 (1998).
29. Putten, M. J. A. M., Tjepkema-Cloostermans, M. C. & Hofmeijer, J. Infraslow EEG activity modulates cortical excitability in postanoxic encephalopathy. *J. Neurophysiol.* **113**, 3256–3267 (2015).
30. Grooms, J. K. *et al.* Infraslow electroencephalographic and dynamic resting state network activity. *Brain Connect.* **7**, 265–280 (2017).
31. Gilden, D. L., Thornton, T. & Mallon, M. W. 1/f noise in human cognition. *Science* **267**, 1837–1839 (1995).
32. Rayshubskiy, A. *et al.* Direct, intraoperative observation of 0.1 Hz hemodynamic oscillations in awake human cortex: Implications for fMRI. *Neuroimage* **87**, 323–331 (2014).
33. Noordmans, H. J. *et al.* Detailed view on slow sinusoidal, hemodynamic oscillations on the human brain cortex by fourier transforming oxy/deoxy hyperspectral images. *Hum. Brain Mapp.* **39**, 3558–3573 (2018).

691 34. Kaällquist, Å. The CSF/Blood Potential in Sustained Acid-Base Changes in the Rat.
692 With Calculations of Electrochemical Potential Differences for H+ and HCO-3. *Acta*
693 *Physiol. Scand.* **78**, 85–93 (1970).
694 35. Sorensen, E., Olesen, J., Rask-Madsen, J. & Rask-Andersen, H. The electrical
695 potential 775 difference and impedance between CSF and blood in unanesthetized man.
696 *Scand J* **776**, 203–207 (1978).
697 36. Voipio, J., Tallgren, P., Heinonen, E., Vanhatalo, S. & Kaila, K. Millivolt-scale DC
698 shifts in the human scalp EEG: evidence for a nonneuronal generator. *J. Neurophysiol.*
699 **89**, 2208–2214 (2003).
700 37. Desjardins, M., Berti, R., Lefebvre, J., Dubeau, S. & Lesage, F. Aging-related
701 differences in cerebral capillary blood flow in anesthetized rats. *Neurobiol. Aging* **35**,
702 1947–1955 (2014).
703 38. Erdő, F., Denes, L. & Lange, E. Age-associated physiological and pathological
704 changes at the blood–brain barrier: A review. *J. Cereb. Blood Flow Metab.* **37**, 4–24
705 (2017).
706 39. Banks, W. A., Reed, M. J., Logsdon, A. F., Rhea, E. M. & Erickson, M. A. Healthy
707 aging and the blood–brain barrier. *Nat. Aging* **1**, 243–254 (2021).
708 40. Babiloni, C. *et al.* Sources of cortical rhythms in adults during physiological aging: A
709 multicentric EEG study. *Hum. Brain Mapp.* **27**, 162–172 (2006).
710 41. Hashemi, A. *et al.* Characterizing population EEG dynamics throughout adulthood.
711 *ENeuro* **3**, (2016).
712 42. Hoshi, H. & Shigihara, Y. Age-and gender-specific characteristics of the resting-state
713 brain activity: A magnetoencephalography study. (2020).
714 43. Kumral, D. *et al.* BOLD and EEG signal variability at rest differently relate to aging in
715 the human brain. *NeuroImage* **207**, 116373 (2020).
716 44. Scally, B., Burke, M. R., Bunce, D. & Delvenne, J. F. Resting-state EEG power and
717 connectivity are associated with alpha peak frequency slowing in healthy aging.
718 *Neurobiol. Aging* **71**, 149–155 (2018).

45. Vysata, O. *et al.* Age-related changes in EEG coherence. *Neurol. Neurochir. Pol.* **48**, 35 (2014).
46. Babayan, A. *et al.* A mind-brain-body dataset of MRI, EEG, cognition, emotion, and peripheral physiology in young and old adults. *Sci. Data* **6**, 1–21 (2019).
47. McFarland, D. J. The advantages of the surface Laplacian in brain–computer interface research. *Int. J. Psychophysiol.* **97**, 271–276 (2015).
48. Huang, Y., Parra, L. C. & Haufe, S. The New York Head—A precise standardized volume conductor model for EEG source localization and tES targeting. *NeuroImage* **140**, 150–162 (2016).
49. Desikan, R. S. *et al.* An automated labeling system for subdividing the human cerebral cortex on MRI scans into gyral based regions of interest. *Neuroimage* **31**, 968–980 (2006).
50. Haufe, S. & Ewald, A. A Simulation Framework for Benchmarking EEG-Based Brain Connectivity Estimation Methodologies. *Brain Topogr.* **32**, 625–642 (2019).
51. Pascual-Marqui, R. D. Discrete, 3D distributed, linear imaging methods of electric neuronal activity. *Part* **1**, (2007).
52. Wen, H. & Liu, Z. Separating fractal and oscillatory components in the power spectrum of neurophysiological signal. *Brain Topogr.* **29**, 13–26 (2016).
53. Tort, A. B., Komorowski, R., Eichenbaum, H. & Kopell, N. Measuring phase-amplitude coupling between neuronal oscillations of different frequencies. *J. Neurophysiol.* **104**, 1195–1210 (2010).
54. Maris, E. & Oostenveld, R. Nonparametric statistical testing of EEG-and MEG-data. *J. Neurosci. Methods* **164**, 177–190 (2007).
55. Aru, J. *et al.* Untangling cross-frequency coupling in neuroscience. *Curr. Opin. Neurobiol.* **31**, 51–61 (2015).
56. Benjamini, Y. & Hochberg, Y. Controlling the false discovery rate: A practical and powerful approach to multiple testing. *J. R. Stat. Soc. Ser. B Methodol.* **57**, 289–300 (1995).

57. Wei, J. *et al.* Eyes-open and eyes-closed resting states with opposite brain activity in sensorimotor and occipital regions: Multidimensional evidences from machine learning perspective. *Front. Hum. Neurosci.* **12**, 422 (2018).
58. Costumero, V., Bueichekú, E., Adrián-Ventura, J. & Ávila, C. Opening or closing eyes at rest modulates the functional connectivity of V1 with default and salience networks. *Sci. Rep.* **10**, 9137 (2020).
59. Leopold, D. A., Murayama, Y. & Logothetis, N. K. Very slow activity fluctuations in monkey visual cortex: Implications for functional brain imaging. *Cereb. Cortex* **13**, 422–433 (2003).
60. Monto, S., Vanhatalo, S., Holmes, M. D. & Palva, J. M. Epileptogenic neocortical networks are revealed by abnormal temporal dynamics in seizure-free subdural EEG. *Cereb. Cortex* **17**, 1386–1393 (2007).
61. Ko, A. L., Darvas, F., Poliakov, A., Ojemann, J. & Sorensen, L. B. Quasi-periodic fluctuations in default mode network electrophysiology. *J. Neurosci.* **31**, 11728–11732 (2011).
62. Davies, P. F. Hemodynamic shear stress and the endothelium in cardiovascular pathophysiology. *Nat. Clin. Pract. Cardiovasc. Med.* **6**, 16–26 (2009).
63. Fisher, A. B., Chien, S., Barakat, A. I. & Nerem, R. M. Endothelial cellular response to altered shear stress. *Am. J. Physiol.-Lung Cell. Mol. Physiol.* **281**, 529–533 (2001).
64. Cucullo, L., Hossain, M., Puvenna, V., Marchi, N. & Janigro, D. The role of shear stress in Blood-Brain Barrier endothelial physiology. *BMC Neurosci.* **12**, 1–15 (2011).
65. Rivadulla, C., Labra, C., Grieve, K. L. & Cudeiro, J. Vasomotion and neurovascular coupling in the visual thalamus in vivo. *PLoS One* **6**, 28746 (2011).
66. Golanov, E. V., Yamamoto, S. & Reis, D. J. Spontaneous waves of cerebral blood flow associated with a pattern of electrocortical activity. *Am. J. Physiol.-Regul. Integr. Comp. Physiol.* **266**, 204–214 (1994).
67. Mitra, A. *et al.* Spontaneous infra-slow brain activity has unique spatiotemporal dynamics and laminar structure. *Neuron* **98**, 297–305 (2018).

68. Weber, C. M. & Clyne, A. M. Sex differences in the blood–brain barrier and neurodegenerative diseases. *APL Bioeng.* **5**, (2021).
69. Dion-Albert, L. *et al.* Sex differences in the blood–brain barrier: Implications for mental health. *Front. Neuroendocrinol.* **65**, 100989 (2022).
70. Zhao, X. *et al.* Wall shear stress in major cerebral arteries as a function of age and gender—A study of 301 healthy volunteers. *J. Neuroimaging* **25**, 403–407 (2015).
71. Zuloaga, K. L., Davis, C. M., Zhang, W. & Alkayed, N. J. Role of aromatase in sex-specific cerebrovascular endothelial function in mice. *Am. J. Physiol.-Heart Circ. Physiol.* **306**, 929–93 (2014).
72. Marlatt, K. L., Kelly, A. S., Steinberger, J. & Dengel, D. R. The influence of gender on carotid artery compliance and distensibility in children and adults. *J. Clin. Ultrasound* **41**, 340–346 (2013).
73. Tanaka, H. *et al.* Aging, habitual exercise, and dynamic arterial compliance. *Circulation* **102**, 1270–1275 (2000).
74. Girouard, H. & Iadecola, C. Neurovascular coupling in the normal brain and in hypertension, stroke, and Alzheimer disease. *J. Appl. Physiol.* **100**, 328–335 (2006).
75. Gursoy-Ozdemir, Y. *et al.* Cortical spreading depression activates and upregulates MMP-9. *J. Clin. Invest.* **113**, 1447–1455 (2004).
76. Meyer, M. F., Rose, C. J., Hülsmann, J. O., Schatz, H. & Pfohl, M. Impairment of cutaneous arteriolar 0.1 Hz vasomotion in diabetes. *Exp. Clin. Endocrinol. Diabetes* **111**, 104–110 (2003).
77. Kadry, H., Noorani, B. & Cucullo, L. A blood-brain barrier overview on structure, function, impairment, and biomarkers of integrity. *Fluids Barriers CNS* **17**, 69 (2020).
78. Smoliński, Ł. & Członkowska, A. Cerebral vasomotor reactivity in neurodegenerative diseases. *Neurol. Neurochir. Pol.* **50**, 455–462 (2016).

Author Contributions: **F.S.**, **A.V.**, and **V.V.N.** conceptualized and designed the study. **F.S.** conducted the literature review, synthesized the literature, computed the analysis and wrote the original draft of the manuscript. **A.V.** and **V.V.N.** supervised the project and provided critical guidance on the manuscript structure. **P.S.** reviewed and validated the code and analytical workflows. **D.K.** contributed to framing the initial manuscript outline and offered conceptual support. **M.G.**, **J.Z.**, **A.V.**, and **V.V.N.** critically reviewed and edited the manuscript. All authors reviewed and approved the final version of the manuscript.

Supplementary Files

This is a list of supplementary files associated with this preprint. Click to download.

- SupplementaryMaterial.pdf